

Blue Microlasers Integrated on a Photonic Platform on Silicon

Farsane Tabataba-Vakili,^{†,‡,§} Laetitia Doyennette,[¶] Christelle Brimont,[¶] Thierry Guillet,[¶] Stéphanie Rennesson,[§] Eric Frayssinet,[§] Benjamin Damilano,[§] Jean-Yves Duboz,[§] Fabrice Semond,[§] Iannis Roland,^{†,¶} Moustafa El Kurdi,[†] Xavier Checoury,[†] Sébastien Sauvage,[†] Bruno Gayral,[‡] and Philippe Boucaud^{*,†,§}

[†]Centre de Nanosciences et de Nanotechnologies, CNRS, Université Paris-Sud, Université Paris-Saclay, F-91405 Orsay, France

[‡]CEA, INAC-PHELIQS, Nanophysique et Semiconducteurs Group, Université Grenoble Alpes, F-38000 Grenoble, France

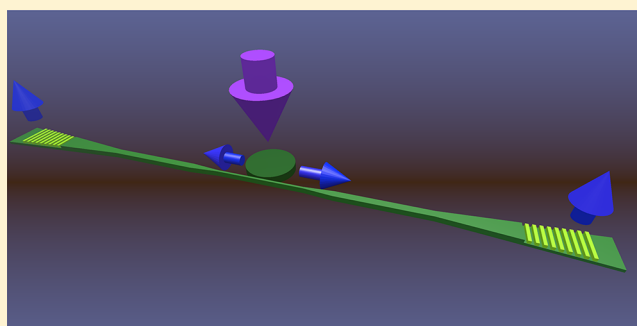
[¶]Laboratoire Charles Coulomb (L2C), Université de Montpellier, CNRS, F-34095 Montpellier, France

[§]Université Côte d'Azur, CRHEA-CNRS, F-06560 Valbonne, France

Supporting Information

ABSTRACT: The main interest of group-III-nitride nanophotonic circuits is the integration of active structures and laser sources. A photonic platform of group-III-nitride microdisk lasers integrated on silicon and emitting in the blue spectral range is demonstrated. The active microdisks are side-coupled to suspended bus waveguides, and the coupled emission is guided and outcoupled to free space using grating couplers. A small gap size of less than 100 nm between the disk and the waveguide is required in the blue spectral range for optimal evanescent coupling. To avoid reabsorption of the microdisk emission in the waveguide, the quantum wells are etched away from the waveguide. Under continuous-wave excitation, loaded quality factors greater than 2000 are observed for the whispering gallery modes for devices with small gaps and large waveguide bending angles. Under pulsed excitation conditions, lasing is evidenced for 3 μm diameter microdisks integrated in a full photonic circuit. We thus present a first demonstration of a III-nitride microlaser coupled to a nanophotonic circuit.

KEYWORDS: microcavity laser, integrated photonic circuit, III-nitride on silicon, whispering gallery mode resonator, microdisk, GaN



In recent years, group-III-nitride on silicon nanophotonics has been a field of considerable interest, as this material system poses a promising platform for photonics. The first asset of III-nitrides is the large transparency window from the near-infrared to the blue and ultraviolet (UV) spectral range.^{1–5} The monolithic integration of active emitters at short wavelength is certainly the most striking second advantage as compared to other photonic platforms. An integrated photonic platform like the one based on indium phosphide (InP) is limited to the near-infrared spectral range.⁶ Both silicon (Si) and silicon nitride (SiN) photonics are lacking efficient integrated active laser emitters. The third advantage of the III-nitride materials for photonics is their possible co-integration with III-nitride electronics, thus offering a complete toolbox for designers. The application domains of III-nitride photonics cover quantum technologies, including emission of entangled photon pairs in the near-infrared,⁷ the optical manipulation of ion-trapped qubits in the UV,⁸ and quantum sensing.^{9,10} Biophotonic applications in the blue and visible spectral ranges, gallium nitride (GaN) being biocompatible,^{11,12} and visible communications with microdis-

plays and light fidelity (Li-Fi) communications¹³ might as well benefit from this platform.

So far, photonic circuits using light emitting diodes (LEDs)¹⁴ and passive photonic circuits using sputtered aluminum nitride (AlN) on oxide^{2,4,15,16} have been demonstrated on silicon substrates. In parallel, there have been numerous reports on single III-nitride microdisk resonators and lasers on silicon and sapphire substrates with quality (Q) factors larger than 10 000.^{17–25} Here we demonstrate the combination of a monolithic blue microlaser emitter with photonic circuitry on silicon. A major difficulty in combining a microdisk laser containing quantum wells (QWs) as the active medium with a waveguide is to avoid reabsorption of the emission in the waveguide. We are tackling this issue by partially etching the waveguide to remove the QWs, which are within 120 nm of the surface. Similar active devices have been fabricated in other material systems with absorbing waveguides,^{26,27} while selective regrowth has also been proposed as a method to avoid reabsorption.²⁸ Another technological

Received: April 25, 2018

Published: July 29, 2018

challenge is achieving the small gap size of less than 100 nm between the disk and the waveguide that is required in the blue spectral range for efficient coupling. Furthermore, the III-nitride photonic circuit must be suspended to avoid absorption in the silicon substrate and to have a good vertical confinement by refractive index contrast to air. We have successfully fabricated suspended active III-nitride photonic circuits containing a microdisk laser, a bus waveguide with a gap size as small as 80 nm, and outcoupling gratings at both ends of the waveguide (see Figure 1). For waveguides with a large bending

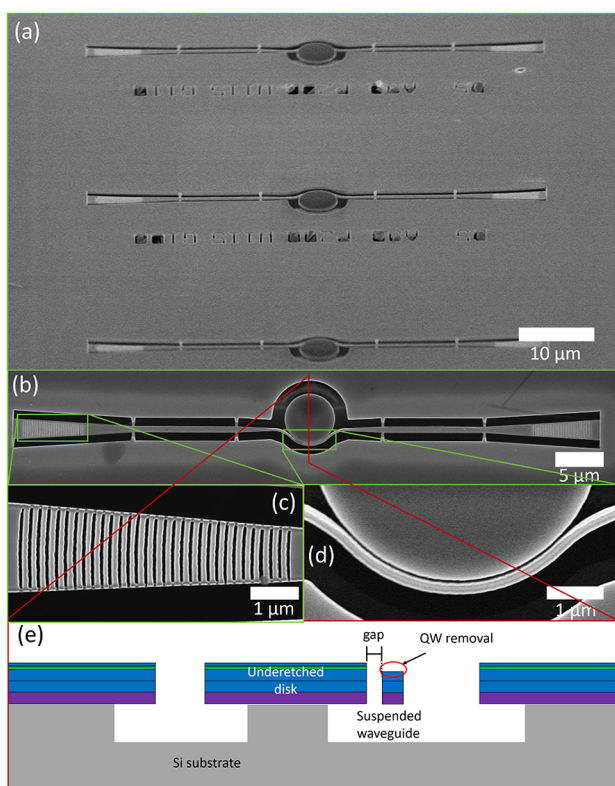


Figure 1. SEM image of III-nitride photonic circuit. (a) View of several devices at an angle, (b) top view of one device, (c) close-up of a grating coupler, (d) close-up of the disk and waveguide coupling region, (e) sketch of a side-view of the fabricated device.

angle around the disk and small gap sizes, we observe large loaded quality factors greater than 2000 under low-power continuous-wave (cw) pumping. For microdisks with larger gaps and straight waveguides, we have observed lasing under pulsed optical pumping conditions from the disk's scattered light and from guided light outcoupled to free space through the gratings.

RESULTS AND DISCUSSION

The investigated sample was grown on a 2 in. silicon(111) substrate using molecular beam epitaxy (MBE). First a buffer layer consisting of 100 nm of AlN, 100 nm of n-doped GaN (silicon concentration of $5 \times 10^{19} \text{ cm}^{-3}$), and 200 nm of undoped GaN was deposited. Then the active region was grown consisting of 10 pairs of 2.2 nm 12% indium gallium nitride ($\text{In}_{0.12}\text{Ga}_{0.88}\text{N}$) QWs and 9 nm GaN barriers.

We hereafter present our technological approach to couple a III-nitride microlaser to an integrated photonic circuit on a silicon platform. Microdisk photonic circuits were fabricated using three levels of electron beam lithography with UV3 resist

(diluted 1:1 with EC solvent) and inductively coupled plasma (ICP) etching using boron trichloride (BCl_3) and chlorine (Cl_2) gases. For each level, plasma-enhanced chemical vapor deposition (PECVD) silicon dioxide (SiO_2) was used as a hard mask during ICP etching. In the first level the microdisk and bus waveguide are defined and the surrounding area is etched to the substrate (a noncontinuous thin AlN layer remains around the microdisks). The QWs are removed selectively from the waveguide in the second level by opening the area containing the previously defined waveguide and etching to a depth of 120 nm. In the third level, the gratings are defined at both ends of the waveguide and etched 200 nm deep. Subsequently, the devices are isotropically underetched by xenon difluoride (XeF_2), in principal leaving the disk with a silicon pedestal and the waveguide and grating suspended. Some of the $3 \mu\text{m}$ disks are suspended without a pedestal through a thin layer of AlN at the foot of the disk. The total device length is $60 \mu\text{m}$ with about $20 \mu\text{m}$ between the edge of the disk and the beginning of the grating. The microdisks are 3 and $5 \mu\text{m}$ in diameter. The bending angle of the waveguide around the disk has been varied between 0° and 90° , where 0° corresponds to a straight waveguide and 90° corresponds to the waveguide being bent around one-quarter of the disk's circumference. The gap size g was varied between 80 and 120 nm and the grating period between 170 and 210 nm. Figure 1a–d show scanning electron microscope (SEM) images of the devices with close-ups of the grating coupler and the disk–waveguide coupling region. Figure 1e shows a schematic cross-sectional view of the device, depicting the disk underetch, waveguide suspension, and the QW removal. More SEM close-ups of different components of the photonic circuit are shown in Figure S10 in the additional microscope and SEM images section in the Supporting Information. A visualization of the top-view of a disk with a 90° bent waveguide and its simulated H_z field, showing the main device parameters, is depicted in Figure S1 in the finite-difference time-domain (FDTD) simulations section in the Supporting Information.

We performed microphotoluminescence ($\mu\text{-PL}$) measurements on these devices using a low-power cw pump laser at 244 nm and a charged couple device (CCD) as the detector in a top-collection setup. Figure 2a shows a 2D map of the CCD, where the vertical axis is the distance along the device direction and the horizontal axis is the wavelength. In the vertical direction 1 pixel on the CCD map corresponds to a distance of $0.9 \mu\text{m}$ on the sample. The vertical position on the CCD is matched with the SEM image next to it (Figure 2b). The central, oversaturated emission comes from the QW luminescence scattered from the center of the microdisk. Faint emission, spatially separated from the high intensity central region can be observed from the grating couplers. Figure S8 in the additional micro-PL results section in the Supporting Information shows a more oversaturated version of Figure 2a to highlight the emission from the gratings. Figure 2c shows spectra integrated over 5 pixels along the vertical axis of the CCD, which corresponds to $4.5 \mu\text{m}$ on the sample. Clear whispering gallery mode (WGM) emission is observed from both gratings, while much higher intensity emission without any visible modes is observed from the center of the disk. The free carrier absorption in the n-doped part of the waveguide is only in the range of 50 cm^{-1} .²⁹ Taking the overlap of the mode with this region (28%) into account, the estimated propagation losses due to doping are negligible. A comparison between experimental and simulated spectra is shown in Figure S2 in

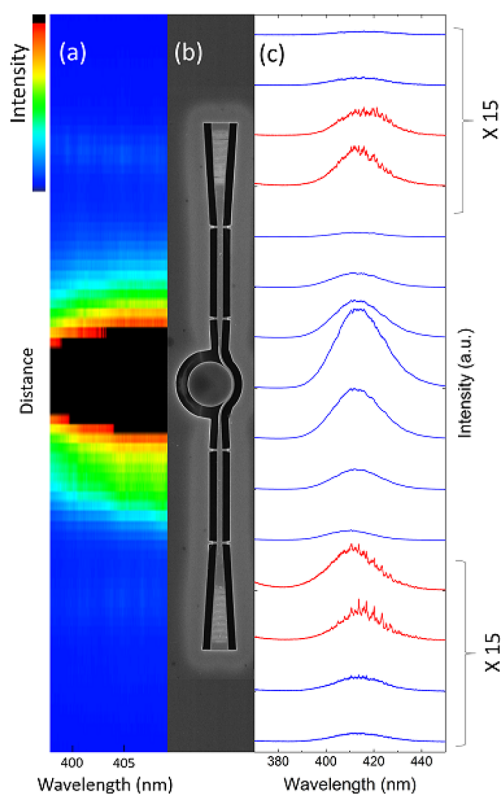


Figure 2. Visualization of the spatial distribution of the emission. (a) 2D intensity map of the CCD, (b) SEM image of the device matched to the CCD image along the vertical axis, (c) spectra integrated over 5 pixels along the vertical axis corresponding to (a) and (b) in vertical position.

the FDTD simulations section in the Supporting Information. This result demonstrates light routing and extraction using an active blue emitter.

μ -PL measurements for different gap sizes and bending angles are shown in Figure 3 for devices with 5 μm diameter disks, integrated spatially over one grating coupler on the CCD. Broad QW luminescence that couples to the waveguide and is outcoupled at the grating is observed in all spectra and decreases in intensity with increasing gap size. WGMs can also be seen in all spectra. Larger contrast WGM resonances are observed for small gaps (Figure 3a) and large angles (Figure 3b), giving loaded Q factors larger than 2000 in the blue, as can be seen in the close-up in Figure 3c. We attribute the sharp resonances with high Q factor to the first-order radial modes. The azimuthal number for the first-order radial mode at 422 nm is 84, according to our FDTD simulations. Lower Q factor broader modes of higher radial order are also detected, indicating the presence of different families of modes. The here-observed WGM contrast (defined as mode intensity divided by background intensity) of up to 2.7 is the largest we have measured for such microdisks in a top-collection setup. In previous measurements, we had to use in-plane side-collection to detect the WGMs directly from the disk, since the modes radiate preferentially in the layer plane.^{20,30} The loaded Q factors are very similar compared to the intrinsic Q factors of individual disks, which we have previously determined to be around 2500 for disks fabricated from the same wafer.³⁰ Figure S6 in the additional micro-PL section in the Supporting Information shows measurements of 3 μm diameter disks with

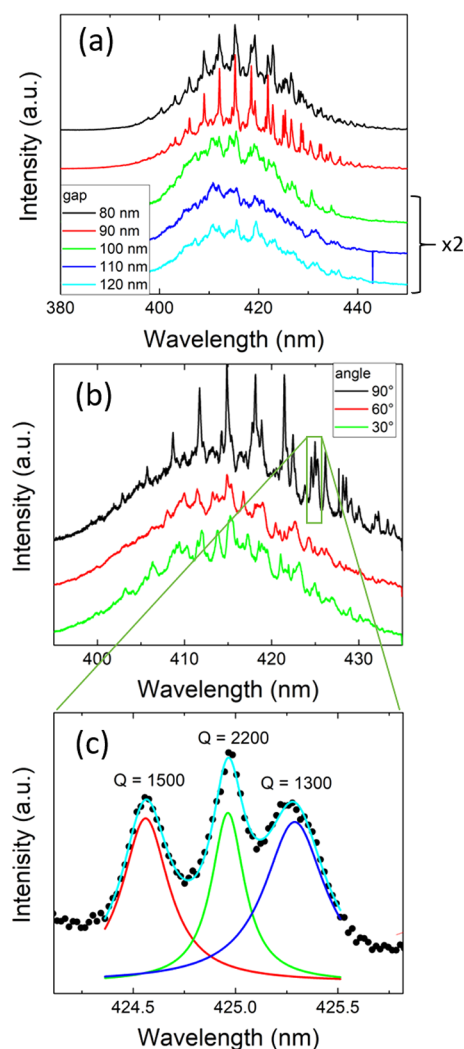


Figure 3. PL measurements integrated over one grating coupler on the CCD for devices with a disk diameter of 5 μm , a waveguide width of 155 nm, and a grating period of 210 nm. (a) The waveguide bending angle is 90° and the gap sizes vary between 80 and 120 nm. The spectra for $g = 100$ –120 nm have been multiplied by 2 for better visibility of the modes. (b) The gap is 90 nm and the bending angle has been varied between 90° and 30°. (c) Close-up of three modes of the 90° spectrum in (b) showing Lorentzian fits and the corresponding Q factors.

90° bent waveguides depicting loaded Q factors in the range of 1200 to 1900.

The loaded Q factor for a disk and side-coupled waveguide is $1/Q_{\text{loaded}} = 1/Q_{\text{int}} + 1/Q_c$, where Q_{int} is the intrinsic Q factor of the disk and Q_c is the coupling Q factor. Q_c depends on the mode overlap between the WGM and the waveguide mode, the interaction length, and the phase mismatch. It is thus dependent on several parameters including the gap distance, the microdisk radius, and the waveguide width. The spatial overlap of the first-order radial mode with the waveguide mode is smaller than the one of higher-order radial modes. As shown by Soltani³¹ for the case of silicon-based coupled resonators, the coupling strength (defined as $1/Q_c$) is usually weaker for the first-order radial modes, thus leading to higher Q_c factors as compared to higher-order radial modes. We mention the term “usually”, as there might be some specific parameter combinations where this assumption does not hold because

of phase mismatch issues. This feature has a strong impact on the mode visibility since the emission coupling to the waveguide depends on the values of Q_{int} and Q_c as for the case of transmission with microdisks and bus waveguides.³²

As the gap distance increases, Q_c will increase exponentially and the fraction of the light transmitted through the waveguide drops very rapidly to zero. According to FDTD modeling (see Figure S3a) in the FDTD simulations section in the Supporting Information), the critical coupling distance is 50 nm for the first-order radial modes, i.e., the ones where $Q_{\text{int}} = Q_c$ and thus $Q_{\text{loaded}} = 1/2Q_{\text{int}}$. For gap distances larger than 80 nm, we are in the undercoupled regime, and the loaded Q factor should increase steadily toward the intrinsic Q factor. However, the coupled intensity decreases. In the case of the 120 nm gap, the first-order radial modes are barely visible in FDTD transmission simulations (see Figure S3a in the FDTD simulations section in the Supporting Information). Meanwhile, the higher-order radial modes have both a lower intrinsic quality factor and a lower coupling quality factor as compared to the first-order radial modes. The amplitude of the higher-order radial modes coupled to the waveguide decreases as well with the gap distance but less sharply than the first-order radial modes. It explains why in Figure 3a the transmission spectra for gaps above 100 nm are dominated by the low Q factor broad modes and that the mode visibility of the first-order radial modes with high Q factor is quenched above 90 nm. Moreover, there is some scattered spontaneous emission from the disk collected above the waveguide, and this background signal decreases the overall visibility of the modes. In future experiments, we will increase the distance between disk and grating to reduce the background signal.

Using a 266 nm laser under pulsed conditions (400 ps, 4 kHz), lasing was observed from devices with 3 μm diameter disks, straight waveguides, and 100 to 120 nm gaps. Figure 4 shows power-dependent measurements both collected close to the disk (Figure 4a) and from the outcoupling grating (Figure 4b) for a device with a gap of 120 nm. The threshold was

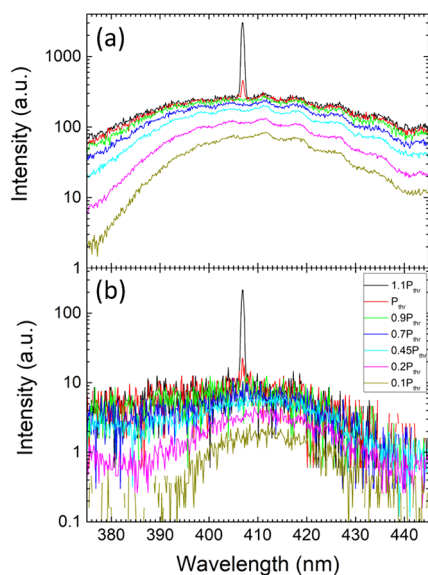


Figure 4. Logarithmic power-dependent pulsed lasing spectra of a device with a 3 μm diameter disk, a straight waveguide, and a 120 nm gap measured (a) above the disk and (b) above the outcoupling grating. The threshold excitation power is $P_{\text{thr}} = 15 \text{ mJ}/\text{cm}^2$ per pulse.

estimated to be $15 \text{ mJ}/\text{cm}^2$ per pulse, and lasing was observed up to our maximum available energy density of $16.5 \text{ mJ}/\text{cm}^2$ per pulse. For individual microdisk lasers with a slightly larger diameter of 4 μm fabricated from the same wafer, we have previously observed thresholds of $3 \text{ mJ}/\text{cm}^2$ per pulse.³⁰ Figure S7 in the additional micro-PL section in the Supporting Information shows an S-shaped increase in lasing mode amplitude and line width narrowing for a 4 μm diameter disk without a waveguide fabricated on the same wafer. The here larger threshold is explained by differences in thermal management and heat dissipation issues due to the lack of a silicon pedestal (see the microscope image in Figure S9a in the additional microscope and SEM images section in the Supporting Information)²⁰ and fluctuations in the processing with increased side-wall roughness and lower Q factors. The lasing mode and broad QW luminescence can be observed from both the disk and the grating. At the disk the emission has a higher intensity, while a factor 2 better contrast between the lasing mode and the QW luminescence is obtained at the grating.

We do not observe lasing from any 5 μm diameter disks, which can be explained by an increase in threshold with increasing disk diameter and a decentralized pedestal near the disk edge causing additional losses. Furthermore, we also do not observe lasing from the devices with 3 μm diameter and 90° bent waveguides due to losses in the pedestal, which is decentralized and near the disk edge in this case.

On the basis of FDTD simulations, we estimate the grating outcoupling efficiency to be 3–7% (as shown in Figure S5 in the FDTD simulations section in the Supporting Information). The highest reported value in the literature for a III-nitride grating coupler in the blue is 9%.⁴ The partial etching of the waveguide increases the coupling strength slightly, as shown by the FDTD simulations in Figure S4 in the FDTD simulations section in the Supporting Information.

An interesting feature is that the lasing observed here is monomode, whereas we previously observed multimode lasing for single uncoupled microdisks.^{24,30} Mode selection is certainly enabled by the presence of the bus waveguide in close proximity with the microdisk, which might be the signature of a mechanism of mode selection involving the global structure (microdisk, waveguide, and tethers). This will be the topic of future investigation. The measurements reported in Figure 4 along with the images shown in Figure 1 and Figure 2 demonstrate the first integrated microlaser in the blue.

Under low-power cw excitation we did not observe any modes from devices with straight waveguides, as seen in Figure 3 for bent waveguides (not shown). This is explained by the weak coupling between the microdisk and the straight waveguide that prevents the observation of modes. The bent geometry increases the interaction length and is known to increase the coupling when we are close to phase matching. This enhanced coupling is illustrated in Figure 3b. The main advantage of the bent geometry is to allow a strong coupling, i.e., a low Q_c value, for larger gap distances as compared to straight waveguides.³³ The observation of the first-order radial modes with straight waveguides thus requires much smaller gap distances that are technologically more difficult to achieve with III-nitrides in the blue. It is furthermore challenging to etch III-nitrides with good verticality and smoothness in small openings. When the microdisk starts to lase, the amplitude becomes significantly stronger and the emission can be more

easily observed after coupling to the waveguide and out-coupling through the grating.

CONCLUSION

We have demonstrated the first blue microlaser integrated into a photonic circuit using III-nitride on silicon. Large loaded Q factors greater than 2000 were observed at the outcoupling grating for devices with small gaps and large waveguide bending angles. Pulsed lasing was observed for devices with large gaps and straight waveguides with a threshold of 15 mJ/cm² per pulse. Further work needs to be done on reducing the lasing threshold, increasing the coupling efficiency, and measuring/lowering transmission losses. The here presented results are an important step in demonstrating the viability of the III-nitride on a silicon nanophotonic platform for real-world applications at short wavelength. A further challenge in making this photonic circuit platform on silicon viable for application is efficient electrical injection in III-nitride microdisks.

ASSOCIATED CONTENT

Supporting Information

The Supporting Information is available free of charge on the ACS Publications website at DOI: 10.1021/acsphotonics.8b00542.

Finite-difference time-domain simulations (critical coupling, phase matching, waveguide height, grating coupler); additional micro-PL results; additional micro-scope and SEM images (PDF)

AUTHOR INFORMATION

Corresponding Author

*E-mail: philippe.boucaud@crhea.cnrs.fr.

ORCID

Farsane Tabataba-Vakili: 0000-0001-5911-7594

Thierry Guillet: 0000-0001-9736-0026

Benjamin Damilano: 0000-0001-7127-4461

Present Address

^{||}Université Paris Diderot-Paris7, F-75013 Paris, France.

Notes

The authors declare no competing financial interest.

ACKNOWLEDGMENTS

This work was supported by Agence Nationale de la Recherche under the MILAGAN convention (ANR-17-CE08-0043-02). This work was also partly supported by the RENATECH network. We acknowledge support by a public grant overseen by the French National Research Agency (ANR) as part of the "Investissements d'Avenir" program: Labex GANEX (Grant No. ANR-11-LABX-0014) and Labex NanoSaclay (reference: ANR-10-LABX-0035). We thank Isabelle Robert-Philip for fruitful discussions.

REFERENCES

- (1) Xiong, C.; Pernice, W. H. P.; Tang, H. X. Low-Loss, Silicon Integrated, Aluminum Nitride Photonic Circuits and Their Use for Electro-Optic Signal Processing. *Nano Lett.* **2012**, *12*, 3562–3568.
- (2) Pernice, W. H. P.; Xiong, C.; Schuck, C.; Tang, H. X. Second harmonic generation in phase matched aluminum nitride waveguides and micro-ring resonators. *Appl. Phys. Lett.* **2012**, *100*, 223501.
- (3) Néel, D.; Roland, I.; Checoury, X.; ElKurdi, M.; Sauvage, S.; Brimont, C.; Guillet, T.; Gayral, B.; Semond, F.; Boucaud, P.

Aluminum nitride photonic crystals and microdisks for ultra-violet nanophotonics. *Adv. Nat. Sci.: Nanosci. Nanotechnol.* **2014**, *5*, 023001.

(4) Stegmaier, M.; Ebert, J.; Meckbach, J. M.; Ilin, K.; Siegel, M.; Pernice, W. H. P. Aluminum nitride nanophotonic circuits operating at ultraviolet wavelengths. *Appl. Phys. Lett.* **2014**, *104*, 091108.

(5) Roland, I.; Zeng, Y.; Checoury, X.; ElKurdi, M.; Sauvage, S.; Brimont, C.; Guillet, T.; Gayral, B.; Gromovy, M.; Duboz, J. Y.; Semond, F.; de Micheli, M. P.; Boucaud, P. Near-infrared III-nitride-on-silicon nanophotonic platform with microdisk resonators. *Opt. Express* **2016**, *24*, 9602–9610.

(6) Smit, M.; et al. An introduction to InP-based generic integration technology. *Semicond. Sci. Technol.* **2014**, *29*, 083001.

(7) Guo, X.; Ling Zou, C.; Schuck, C.; Jung, H.; Cheng, R.; Tang, H. X. Parametric down-conversion photon-pair source on a nanophotonic chip. *Light: Sci. Appl.* **2017**, *6*, e16249.

(8) Leonardis, F. D.; Soref, R. A.; Soltani, M.; Passaro, V. M. N. Broadband biphoton generation and statistics of quantum light in the UV-visible range in an AlGaIn microring resonator. *Sci. Rep.* **2017**, *7*, 11387.

(9) Grosso, G.; Lienhard, B.; Moon, H.; Scarabell, D.; Schroeder, T.; Jeong, K.-Y.; Lu, T.-J.; Berhane, A. M.; Wind, S.; Aharonovich, I.; Englund, D. Quantum Emission from Atomic Defects in Wide-Bandgap Semiconductors. *Photonics Society Summer Topical Meeting Series (SUM), IEEE* **2017**, 103–104.

(10) Berhane, A. M.; Jeong, K.-Y.; Bodrog, Z.; Fiedler, S.; Schröder, T.; VicoTriviño, N.; Palacios, T.; Gali, A.; Toth, M.; Englund, D.; Aharonovich, I. Bright Room-Temperature Single-Photon Emission from Defects in Gallium Nitride. *Adv. Mater.* **2017**, *29*, 1605092.

(11) Jewett, S. A.; Makowski, M. S.; Andrews, B.; Manfra, M. J.; Ivanisevic, A. Gallium nitride is biocompatible and non-toxic before and after functionalization with peptides. *Acta Biomater.* **2012**, *8*, 728–733.

(12) Hofstetter, M.; Howgate, J.; Schmid, M.; Schoell, S.; Sachsenhauser, M.; Adigüzel, D.; Stutzmann, M.; Sharp, I. D.; Thalhammer, S. In vitro bio-functionality of gallium nitride sensors for radiation biophysics. *Biochem. Biophys. Res. Commun.* **2012**, *424*, 348–353.

(13) Chi, Y.-C.; Hsieh, D.-H.; Lin, C.-Y.; Chen, H.-Y.; Huang, C.-Y.; He, J.-H.; Ooi, B.; DenBaars, S. P.; Nakamura, S.; Kuo, H.-C.; Lin, G.-R. Phosphorous Diffuser Diverged Blue Laser Diode for Indoor Lighting and Communication. *Sci. Rep.* **2016**, *5*, 18690.

(14) Shi, Z.; Gao, X.; Yuan, J.; Zhang, S.; Jiang, Y.; Zhang, F.; Jiang, Y.; Zhu, H.; Wang, Y. Transferrable monolithic III-nitride photonic circuit for multifunctional optoelectronics. *Appl. Phys. Lett.* **2017**, *111*, 241104.

(15) Pernice, W. H.; Xiong, C.; Tang, H. X. High Q micro-ring resonators fabricated from polycrystalline aluminum nitride films for near infrared and visible photonics. *Opt. Express* **2012**, *20*, 12261–12269.

(16) Xiong, C.; Pernice, W. H. P.; Sun, X.; Schuck, C.; Fong, K. Y.; Tang, H. X. Aluminum nitride as a new material for chip-scale optomechanics and nonlinear optics. *New J. Phys.* **2012**, *14*, 095014.

(17) Tamboli, A. C.; Haberer, E. D.; Sharma, R.; Lee, K. H.; Nakamura, S.; Hu, E. L. Room-temperature continuous-wave lasing in GaN/InGaIn microdisks. *Nat. Photonics* **2007**, *1*, 61–64.

(18) Simeonov, D.; Feltin, E.; Bühlmann, H.-J.; Zhu, T.; Castiglia, A.; Mosca, M.; Carlin, J.-F.; Butté, R.; Grandjean, N. Blue lasing at room temperature in high quality factor GaN/AlInN microdisks with InGaIn quantum wells. *Appl. Phys. Lett.* **2007**, *90*, 061106.

(19) Simeonov, D.; Feltin, E.; Altoukhov, A.; Castiglia, A.; Carlin, J.-F.; Butté, R.; Grandjean, N. High quality nitride based microdisks obtained via selective wet etching of AlInN sacrificial layers. *Appl. Phys. Lett.* **2008**, *92*, 171102.

(20) Mexis, M.; Sergent, S.; Guillet, T.; Brimont, C.; Bretagnon, T.; Gil, d. F. S.; Leroux, M.; Nel, D.; David, S.; Chcoury, X.; Boucaud, P. High quality factor nitride-based optical cavities: microdisks with embedded GaN/Al(GaN) quantum dots. *Opt. Lett.* **2011**, *36*, 2203–2205.

(21) Aharonovich, I.; Woolf, A.; Russell, K. J.; Zhu, T.; Niu, N.; Kappers, M. J.; Oliver, R. A.; Hu, E. L. Low threshold, room-temperature microdisk lasers in the blue spectral range. *Appl. Phys. Lett.* **2013**, *103*, 021112.

(22) Athanasiou, M.; Smith, R.; Liu, B.; Wang, T. Room temperature continuous-wave green lasing from an InGaN microdisk on silicon. *Sci. Rep.* **2015**, *4*, 7250.

(23) Zhang, Y.; Zhang, X.; Li, K. H.; Cheung, Y. F.; Fengand, C.; Choi, H. W. Advances in III-nitride semiconductor microdisk lasers. *Phys. Status Solidi A* **2014**, *210*, 960–973.

(24) Sellés, J.; Brimont, C.; Cassabois, G.; Valvin, P.; Guillet, T.; Roland, I.; Zeng, Y.; Checoury, X.; Boucaud, P.; Mexis, M.; Semond, F.; Gayral, B. Deep-UV nitride-on-silicon microdisk lasers. *Sci. Rep.* **2016**, *6*, 21650.

(25) Rousseau, I.; Callsen, G.; Jacopin, G.; Carlin, J.-F.; Butté, R.; Grandjean, N. Optical absorption and oxygen passivation of surface states in III-nitride photonic devices. *J. Appl. Phys.* **2018**, *123*, 113103.

(26) Koseki, S.; Zhang, B.; Greve, K. D.; Yamamoto, Y. Monolithic integration of quantum dot containing microdisk microcavities coupled to air-suspended waveguides. *Appl. Phys. Lett.* **2009**, *94*, 051110.

(27) Schmidt, G.; Rieger, T.; Trellenkamp, S.; Grütmacher, D.; Pawlis, A. Photon guiding characteristics of waveguide membranes coupled to a microdisk of ZnSe/(Zn,Mg)Se quantum well structures. *Semicond. Sci. Technol.* **2017**, *32*, 075015.

(28) Matsuo, S.; Shinya, A.; Kakitsuka, T.; Nozaki, K.; Segawa, T.; Sato, T.; Kawaguchi, Y.; Notomi, M. High-speed ultracompact buried heterostructure photonic-crystal laser with 13 fJ of energy consumed per bit transmitted. *Nat. Photonics* **2010**, *4*, 648–654.

(29) Kioupakis, E.; Rinke, P.; Schleife, A.; Bechstedt, F.; VandeWalle, C. G. Free-carrier absorption in nitrides from first principles. *Phys. Rev. B: Condens. Matter Mater. Phys.* **2010**, *81*, No. 241201(R), DOI: [10.1103/PhysRevB.81.241201](https://doi.org/10.1103/PhysRevB.81.241201).

(30) Sellés, J.; Crepel, V.; Roland, I.; Kurdi, M. E.; Checoury, X.; Boucaud, P.; Mexis, M.; Leroux, M.; Damilano, B.; Rennesson, S.; Semond, F.; Gayral, B.; Brimont, C.; Guillet, T. III-Nitride-on-silicon microdisk lasers from the blue to the deep ultra-violet. *Appl. Phys. Lett.* **2016**, *109*, 231101.

(31) Soltani, M. Novel Integrated Silicon Nanophotonic Structures using Ultra-high Q Resonators. Ph.D. thesis, Georgia Institute of Technology, 2009.

(32) Yariv, A. Universal relations for coupling of optical power between microresonators and dielectric waveguides. *Electron. Lett.* **2000**, *36*, 321–322.

(33) Hu, J.; Carlie, N.; Feng, N.-N.; Petit, L.; Agarwal, A.; Richardson, K.; Kimerling, L. Planar waveguide-coupled, high-index-contrast, high-Q resonators in chalcogenide glass for sensing. *Opt. Lett.* **2008**, *33*, 2500–2502.